Illumination invariance and shadow compensation via spectro-polarimetry technique

Izzati Ibrahim*, Peter Yuen, Kan Hong, Tong Chen, Umair Soori, James Jackman, Mark Richardson

Department of Informatics and Systems Engineering, Cranfield University, Defence Academy of the UK, Shrivenham, Swindon, SN6 8LA

*email: i.ibrahim@cranfield.ac.uk

Abstract

A major problem for obtaining target reflectance via hyperspectral imaging systems is the presence of illumination and shadow effects. These factors are common artefacts, especially when dealing with a hyperspectral imaging system that has sensors in the visible to near infrared region. This region is known to have highly scattered and diffuse radiance which can modify the energy recorded by the imaging system. Shadow effect will lower the target reflectance values due to the small radiant energy impinging on the target surface. Combined with illumination artefacts, such as diffuse scattering from the surrounding targets, background or environment, the shape of the shadowed target reflectance will be altered. In this study we propose a new method to compensate for illumination and shadow effects on hyperspectral imageries by using a polarization technique. This technique, called spectro-polarimetry, estimates the direct and diffuse irradiance based on two images, taken with and without a polarizer. The method is evaluated using a spectral

similarity measure, angle and distance metric. The results of indoor and outdoor tests have shown that using the spectro-polarimetry technique can improve the spectral constancy between shadow and full illumination spectra.
Keywords: hyperspectral, polarizer, illumination invariance, shadow

1. Introduction

Hyperspectral imaging system (HSI) uses a spectrometry technique to record the electromagnetic energy from the visible to middle or far infrared region. The energy is captured in a narrow slice of wavebands of approximately 5-20 nm. Each recorded pixel in each waveband contains the spatial and spectral information that can be extracted as target reflectance or signature as a function of wavelength. The radiometric properties can be used for target classification or identification on hyperspectral imageries (1). HSI has been employed extensively in all applications, such as agriculture (2, 3), surveillance (4), remote sensing (5, 6), medical (7, 8) and military (9).

HSI system records energy that is reflected or emitted from an object in the scene. Within the visible to near infrared region object surface reflectance dominates the sensor analysis, whereas emissivity is captured in the infrared region. Atmospheric effects, such as scattering and absorption, negatively impact the accuracy of target reflectance or signature. This is especially true for long range applications at a distance of a hundred meters or more. The transmission of an illumination source through the atmosphere can be scattered, absorbed or reflected. This is due to atmospheric aerosol, smog or

smoke particles and the amount is dependent on wavelength (10). This atmospheric modulation also distorts the energy that is reflected by objects in the scene and background, resulting in a mixture of direct and diffuse irradiance entering the sensor. It has been reported that scattering and absorption from gases and particles in the atmosphere are predominant factors that may complicate the target reflectance accuracy (11).

Determination of target reflectance is also complicated by shadow. Regions of shadow occur when a direct source is blocked by an object. The reflected energy recorded by the HSI system from the target under shadow would be a low non-zero reflectance. This low non-zero value is due to the diffuse irradiance scattered by the adjacent targets or background that impinges on the target under shadow. If a multiple mixture of diffuse irradiance exists in the scene, the reflectance of target under shadow would not only have a lower reflectance value, but also a change in its reflectance shape compared to target under direct illumination.

Much research has been conducted to prove that the interpretation of target reflectance is strongly dependent on the illumination of a scene (12). Atjay et al. have shown that the shadow cast by cloud introduced a distortion to target reflectance in the visible region, thus leading to an error in the Normalised Vegetation Index (NDVI) (13). Ibrahim et al. showed that shadow and illumination artefacts can lead to an error in classification by up to 30% (14). The diminished reflectance by a target under shadow can reduce the contrast

between targets and background leading to an error in target detection and classification (15).

A large amount of research has also been reported for illumination invariance and shadow compensation on hyperspectral imageries. Band ratio and normalization techniques were the first approaches introduced (16, 17). These techniques are simple but strongly dependent on the variation of targets in the image. Proper selection of bands is also important for target or background enhancement. Boardman has introduced linear and nonlinear unmixing for shadow correction. In order to overcome shadow effects the choice of endmembers should be selected properly for better shadow pixel characterization (18, 19). The latest work has been reported by Friman et al. for illumination and shadow compensation on hyperspectral imageries (20). This work segments the illumination invariance map using the Digital Surface Model (DSM) generated from an airborne LIDAR (Light Detection and Ranging). Upon the establishment of the map, the shadow pixel is identified and corrected using the non-linear squares estimation. Another approach uses matched filter (MF) detection (21, 22 and 23). This technique calculates the covariance of the image for background characterization and locates the dark pixels on the scene. This work will be compared with the MF technique proposed by Richter which has been employed together with ATCOR atmospheric correction modelling (24).

Most of the research mentioned above compensates for shadow and illumination invariance based on image processing. In this research we

propose a new technique of shadow compensation for hyperspectral images by employing a mixture of hardware and image processing. The hardware method is based on the polarization of a HSI system, known as spectro-polarimetry technique. Our focus is on the hyperspectral images that are illuminated by a single direct source primarily the sun and diffuse sources from the surrounding targets and environment. In this work we employ Spectral Angle Mapper (SAM) algorithm to differentiate between shadow and full illumination pixels. SAM measures the angle for each pixel for all bands between the non-polarized and polarized images. These values represent the state of polarization across the images. This map is then used for correcting for illumination invariance and shadow pixels on hyperspectral imageries.

The polarization technique has been used widely in standard (non-hyperspectral) image processing. The earliest work investigated separating the diffuse and specular components of reflection from an objects surface (25, 26). This technique was developed to improve the colour and intensity of a targets surface. Lin et al. developed a method to work with a polarization sensitive camera to separate shadows from different sources in colour images (27). For hyperspectral imaging systems the polarization technique is fairly new. Wellems and Bowers have reported that the polarization technique has improved the target spectro-polarimetric signatures (28). This achievement can lead to better separation of target signatures and thus enhanced hyperspectral image classification accuracy.

2. Target Reflectance Model

The irradiance of an object is defined as the radiation energy per unit time (power) impinging on the surface, normalized to the surface area (Wm^{-2}) (29). Radiance is the normalization of irradiance to the solid angle of the observation of the reflected light ($Wm^{-2}sr^{-1}$) (29). In any hyperspectral application the target reflectance or signature is the property of interest. Based on Figure 1, given the sun as the source of illumination, the illumination spectral power distribution, E ($Wm^{-2}sr^{-1}$) is expressed as,

$$E = S_\lambda \cos\phi_i \tag{1}$$

For this equation, S_λ is the solar spectral irradiance ($Wm^{-2}sr^{-1}$) and ϕ_i is solar zenith angle. When the source radiation hits the surface the bidirectional reflectance distribution function (BRDF) is given as the ratio of the reflected radiance to incident irradiance,

$$BRDF(sr^{-1}) = \frac{L_\lambda(\theta_r,\phi_r)(W/m^2)}{E_\lambda(\theta_i,\phi_i)(W/m^2 sr)} \tag{2}$$

The relationship between the target reflectance, ρ and *BRDF* is given by,

$$\rho_\lambda(\theta_i,\phi_i,\theta_r,\phi_r) = \pi BRDF(\theta_i,\phi_i,\theta_r,\phi_r) \tag{3}$$

Combining equation 1, 2 and 3, the target reflectance is expressed as:

$$\rho_\lambda = \frac{\pi L_\lambda}{S_\lambda \cos\phi_i} \tag{4}$$

The radiation from sun or any light is expected to be unpolarized. However, when the angle between the incident direction of the light and the normal to the surface becomes smaller, the reflected irradiance becomes partially polarized (30). This research utilizes this information by using the spectro-

polarimetry technique to separate the direct and diffuse irradiance form target reflectance to compensate for illumination and shadow effects.

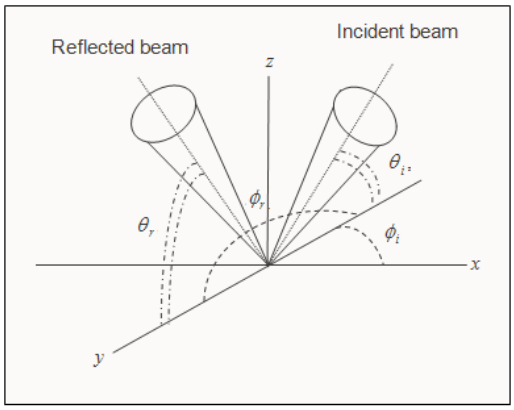

Figure 1 Depiction of the BRDF nomenclature (10).

The surface of targets will reflect the incident radiation partially in the form of direct reflectance and partially in the form of diffuse reflectance, regardless of the direction of the incoming light (31), illustrated in Figure 2. Direct reflectance occurs when the angle of reflected radiation is normal to the incident radiation and is reflected in only a single direction (32). This type of reflectance is sometimes called perfect specular reflectance. Shiny surfaces, such as mirror-like surfaces, have high specular reflectance which will also be highly polarized. Diffuse reflectance relates to scattered light where the irradiation is reflected in many angles (33). If the reflected angles are equal in all directions then the surface is termed a Lambertian source (34). Objects such as paints, cloths and wood that are not shiny are examples of Lambertian surfaces (10). Diffuse surfaces, or groups of objects that have highly scattered reflectance, will have low polarized reflectance.

Some reflected energy from the ground, either direct or diffuse, may influence the pixel quality as recorded by the HSI system in two ways. One is by energy diffusely scattered by the ground and environment to the sensors field of view. The second is the light diffusely scattered by adjacent objects to the targets, then reflected upward to the sensors field of view, which is called sky radiance. Only direct reflectance is of importance for retrieving accurate target reflectance.

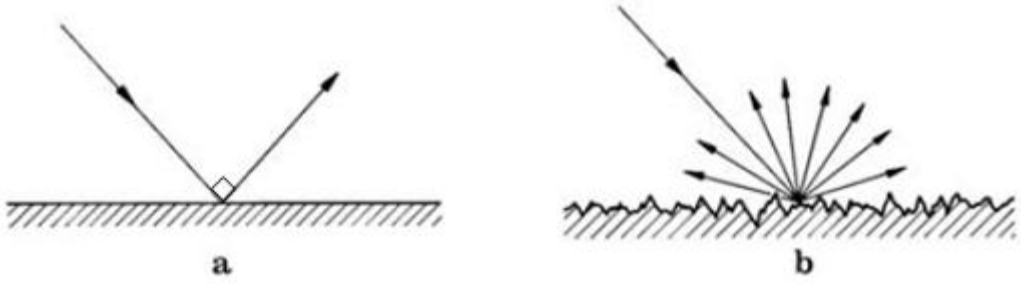

Figure 2 (a) Specular and (b) diffuse reflection (35).

The amount of illumination received by an area can also be reduced due to shadow effects (36). Shadows may be caused by clouds or any obstacles that block the illumination from hitting the target surface. The sensor detects very small non zero reflectance values from targets under shadow due to diffuse irradiance from adjacent targets, background or environment. Edward et al reported that shadow effects do not simply lower the reflectance energy; they also cause a change in the reflectance spectral shape (37). This phenomenon depends on the surroundings that scatter the reflected energy onto the sensors field of view. For scenes that contain uniform background the shape alteration of the shadowed target is not an issue. However, for a scene that contains high variations in targets, the shape alteration appears to be dominant. For hyperspectral target classification and identification, the

reflectance values and shape are of importance. Both should be corrected to avoid an error in target classification and identification.

3. Description of Method

All light consists of two wave components that are orthogonal in the plane perpendicular to the direction of light. By transmitting the light through a linear polarizer, the magnitudes of these properties can be measured. This paper presents a new method for illumination invariance and shadow compensation on hyperspectral imageries, based on a polarization technique called spectro-polarimetry. The technique involves placing an absorptive polarizer filter at the front of the HSI system which absorbs the highly polarized radiation from direct target reflectance (38).

The polarization technique was first used for stellar and planetary astronomy applications (39). It has been extended to colour constancy on RGB images where the polarizer is used to model the reflected radiance distribution of a target (40). Currently, lots of conventional cameras have been fitted with a polarizer filter to improve image quality, such as reducing sky light effect or glare. Polarized sun glasses are also common and help to minimize the suns reflectance entering our eyes.

3.1 Illumination invariance and shadow compensation

Two images taken at the same time with and without the polarizer are denoted by I_{NP} and I_P. Let x be the pixel vector for images I_{NP} and I_P for N bands, then the Spectral Angle Mapper (SAM) algorithm is given by,

$$SAM(x) = \cos^{-1}\left(\frac{\sum_{n}^{N} I_{NP}(x)_n I_P(x)_n}{\left[\sum_{n}^{N} I_{NP}^2(x)_n\right]^{1/2}\left[\sum_{n}^{N} I_P^2(x)_n\right]^{1/2}} \right) \quad \text{where n = band 1,...,N} \qquad (5)$$

SAM measures the angle between the non-polarized image, I_{NP}, to the polarized image, I_P. This value is scaled to be between 0 and 1 using the equation,

$$Scaled\_SAM(x) = 1 - \frac{SAM(x) - \min(SAM)}{\min(SAM) - \max(SAM)} \qquad (6)$$

Scaled_SAM map represent the polarization state on the image. The shadow pixels are corrected by normalizing the shadow image with the Scaled_SAM values and adding the polarized values,

$$Corrected\_shadow_{x,n} = \frac{imageNP_{x,n}}{Scaled\_SAM_x} + \left(imageNP_{x,n} - imageP_{x,n}\right) \qquad (7)$$

3.2 Correction assessment

To assess the effectiveness of the correction method angle and distance similarity metrics are used. Given 2 spectra vector, v_1 and v_2 , the angle similarity metric can be defined as (41),

$$angle(v_1, v_2) = \cos^{-1}\left(\frac{\sum_{n}^{N} v_{1,n} v_{2,n}}{\left[\sum_{n}^{N} v_{1,n}^2\right]^{1/2} \left[\sum_{n}^{N} v_{2,n}^2\right]^{1/2}} \right) \quad \text{where n = band 1,...,N} \qquad (8)$$

A small angle represents the closeness of match between the two spectra and shows the spectral shape similarities of the two vectors. The second assessment is a distance measure and is given by (41),

$$dist(v_1, v_2) = \left[\sum_{n}^{N} (v_{1,n} - v_{2,n})^2\right]^{1/2} \quad \text{where n = band 1,...,N} \qquad (9)$$

4. Equipment and data set

Two sets of data, indoor and outdoor, are taken with and without the polarizer filter. A Headwall VNIR hyperspectral camera is used which has a spectral sensitivity between 400 and 1000 nm; camera shown in Figure 3. The camera employs a diffraction grating as a spectrograph and the polarizer filter is placed on the lens of the camera, seen in Figure 4.

Figure 5 (a) shows the illumination source for the indoor data and (b) 4 different coloured t-shirts imaged in the lab with predominantly white and yellow walls. The light was shinning on the left of the image and the t-shirts are block by an object on the left to cast the shadow. The outdoor data, namely Field Data and Bunker Data shown in Figure 6 and Figure 7, was taken on a clear and sunny day. Calibrated panels, white and black spectralons, are placed in indoor and outdoor data to estimate the irradiance of the scene, shown in Figure 8. All the data used in this research is converted

to ‘apparent’ reflectance using the Empirical Line Method (ELM). The word ‘apparent’ used in the ELM approach does not consider other possible effects, such as topography of the scene, in estimating the targets reflectance. Given at sensor radiance image as L, and the recorded brightness or digital number DN, the linear equation for reflectance conversion is given by (10),

$$L = c_0 + c_1 DN \tag{10}$$

Where c_o and c_1 are the calibration coefficients, measured from the black and white spectralons that are placed in the scene.

Figure 3 The Headwall Visible Near Infra-red (VNIR) imaging system.

Figure 4 The polarizer is placed on the camera lens.

(a) (b)

Figure 5 (a) illumination from the left side of the image and (b) the shadow cast on the t-shirt data.

Figure 6 The outdoor field data taken during midday on sunny day.

Figure 7 The outdoor bunker data taken during midday on sunny day.

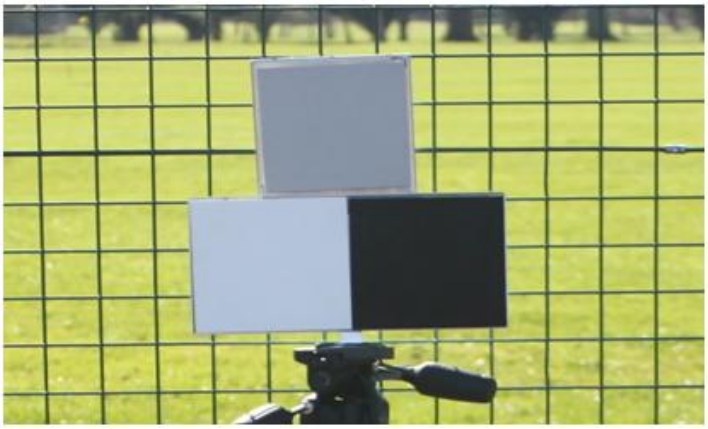

Figure 8 The calibrated panel used in this research.

5. Results

The main objective for this method is to compensate for illumination invariance and shadow effects on hyperspectral imageries. Figure 9 (a) shows the RGB image before correction, (b) the scaled_SAM result between vectors of image I_{NP} and I_P for the indoor scene and (c) the RGB image after correction. Based on the Scaled_SAM map, the shadow area (denoted in blue scale) can easily be detected using the SAM algorithm. The illumination

invariance of the blue t-shirt (on the right of the image), is also detected by SAM. The RGB images shown in this paper are false colour images generated from the red, green and blue wavelengths. Figure 10 shows the plots of reflectance versus wavelength for the 4 t-shirts to compare the reflectance of shadow pixels before and after correction to the direct spectra. The corrected spectra (green curves) have improved and are almost consistent with the direct spectra for all t-shirt colours. The angle and distance similarities for all 4 t-shirt data with comparison to direct reflectance are given in Table 1. Based on the angle similarities in Table 1, the metric for t-shirt classes 3 and 4 are higher after correction due to high polarization within 450 to 550 nm bands. This can be seen by referring to Figure 10 where the shadow reflectance after correction is skewed within this band.

In order to evaluate the inter-separability of target spectra after the correction the Maximum Likelihood (QD) classifier has been used, with the direct spectra as the training data. Figure 11 shows the QD result (a) before and (b) after the shadow correction compared to (c) the target map. The target map is generated from the image that has no shadow effects and the accuracy is calculated using the following equation,

$$Accuracy\% = (PN - PN - NP)\frac{100}{N} \tag{11}$$

PP, PN, NP and N are positive-positive, positive-negative, negative-positive and the total number pixels in the class respectively. It can be seen that the QD result after correction has achieved a better accuracy (98%) compared to the QD result before correction (48%). This result proves the enhanced inter-class separation of targets after the shadow correction.

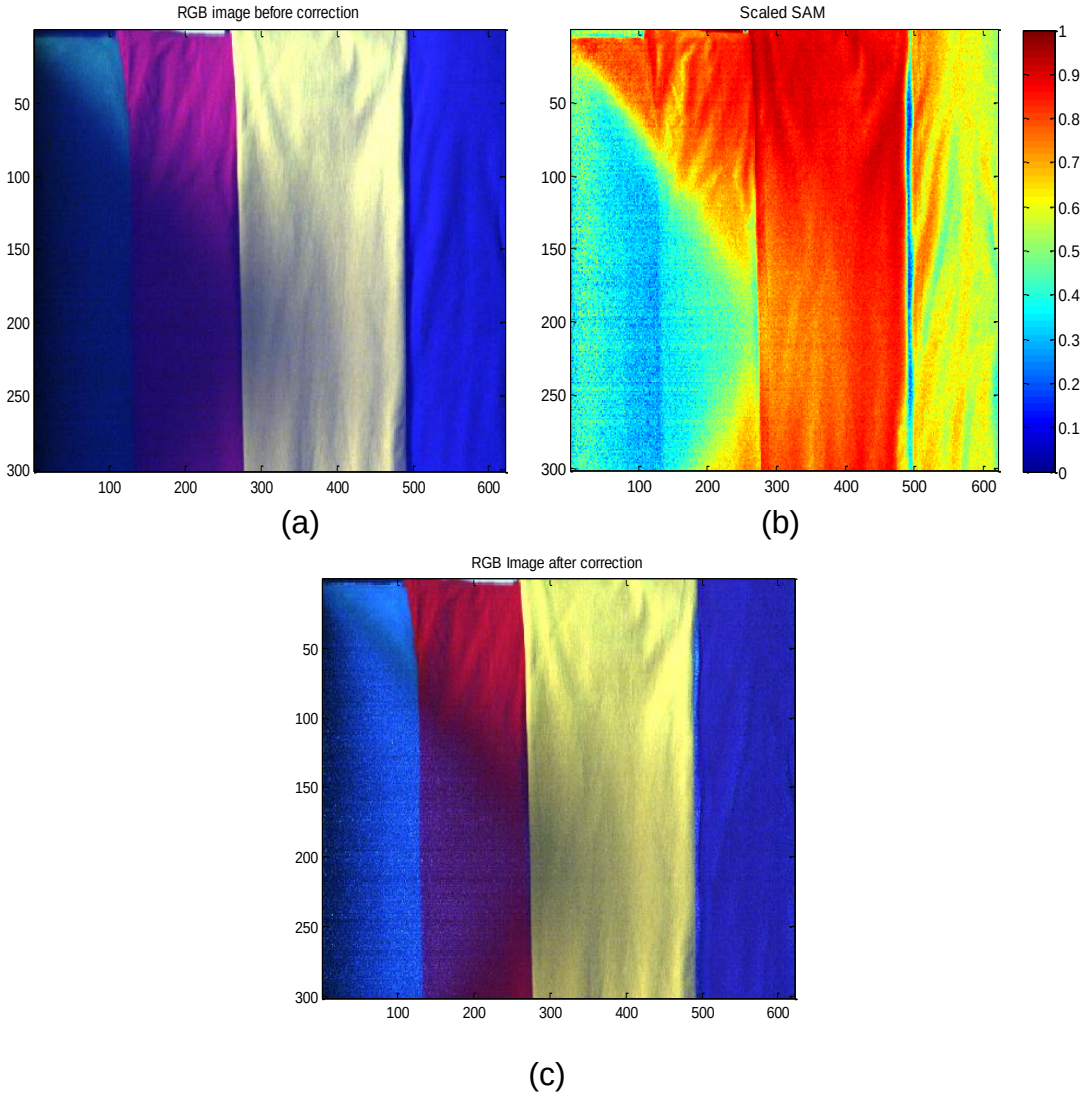

Figure 9 (a) the RGB image before correction, (b) the scaled_SAM result between vectors of image I_{NP} and I_P and (c) RGB image after correction.

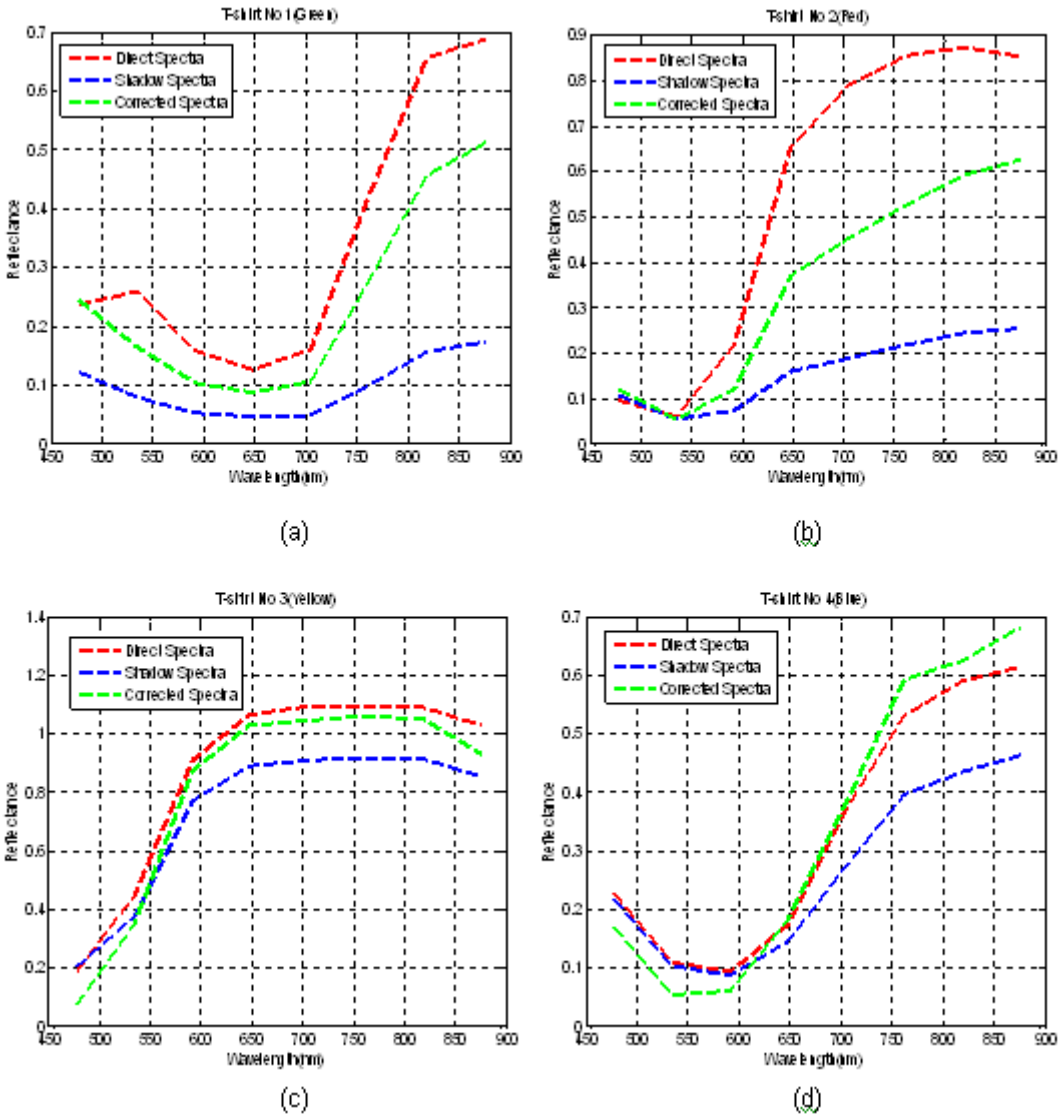

Figure 10 Comparison of shadow spectra before and after correction to the full illumination spectra for (a) t-shirt 1 (Green), (b) t-shirt 2 (Red), (c) t-shirt 3 (Yellow) and (d) t-shirt 4 (Blue).

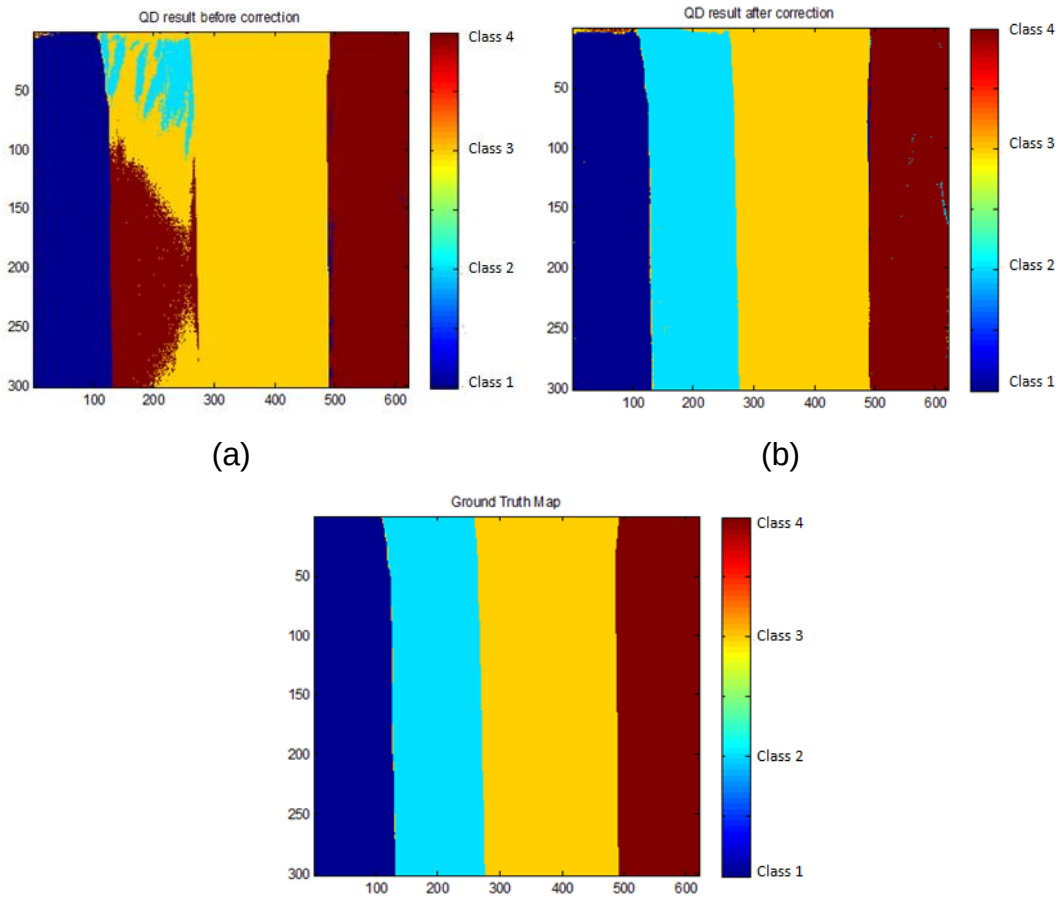

Figure 11 Show the QD result (a) before correction with accuracy 48%, (b) after correction 98% and comparison to (c) the ground truth image.

Table 1 Spectra similarity of shadow reflectance before and after correction with respect to full illumination spectra for indoor data.

Indoor Data	Angle		Distance	
	Before correction	After correction	Before correction	After correction
Green	0.1846	0.0958	0.2622	0.1220
Red	0.0880	0.0492	0.3371	0.1680
Yellow	0.0305	0.0588	0.2217	0.1236
Blue	0.0718	0.0968	0.0969	0.0567

The method proposed shows good consistency on the outdoor *Field* data, seen in Figure 12, where the SAM algorithm is able to detect the shadow pixels between vector image I_{NP} and I_P. The shadow reflectance has improved significantly after the correction, shown in Figure 12 (d). This experiment has been compared to the work proposed by Ritcher for shadow correction on hyperspectral images. Table 2 shows the spectral similarities for before correction, after correction via spectro-polarimetry technique and after correction via matched filter (MF) technique proposed by Ritcher. From the table the spectro-polarimetry technique and matched filter (MF) technique have shown an enhancement for target spectra under shadow region compared to the direct spectra. The spectro-polarimetry technique shows better similarities in angle and distance metric to direct spectra in comparison to the MF technique. This work has also been repeated for other outdoor Bunker data. Figure 13 shows the result of target spectra before and after correction.

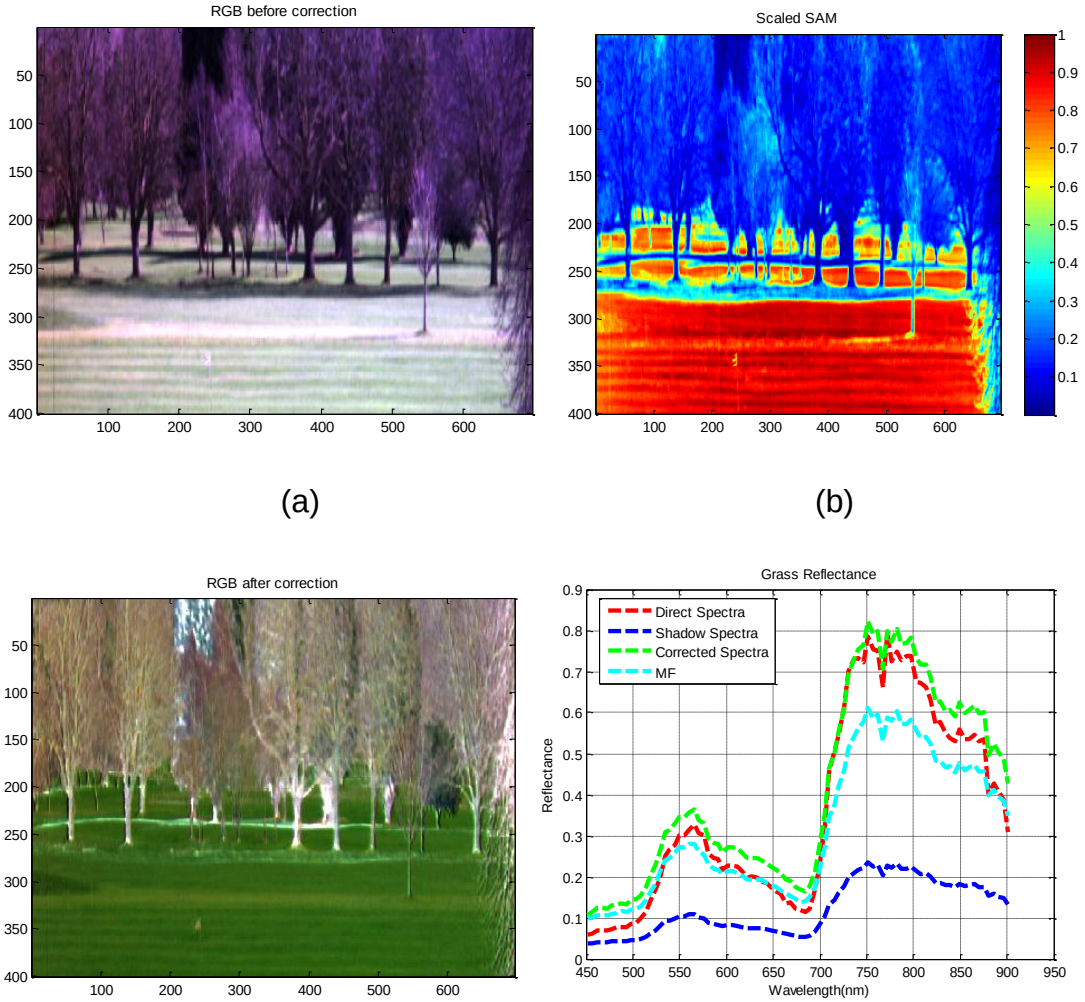

Figure 12 (a) the RGB image before correction (I_{NP}), (b) scaled_SAM result, (c) the RGB after correction and (d) the plot of shadow spectra before and after correction with respect to direct spectra.

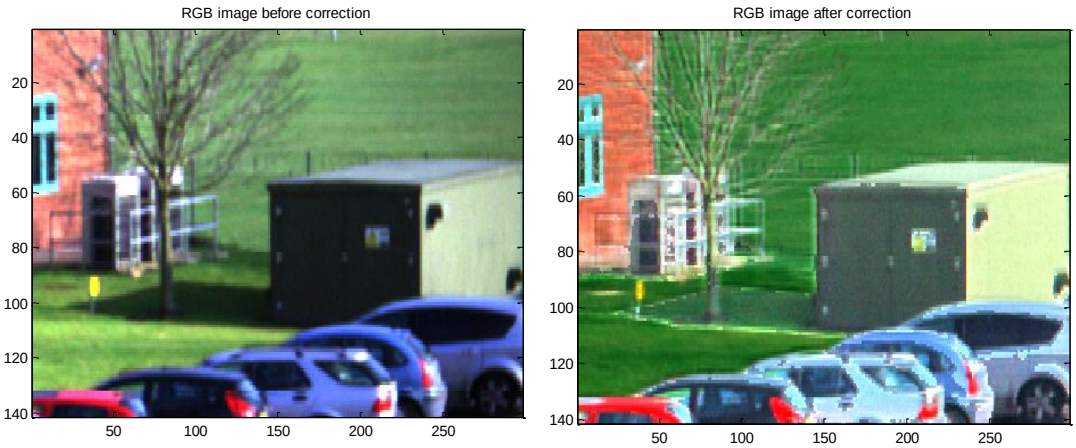

(a) (b)

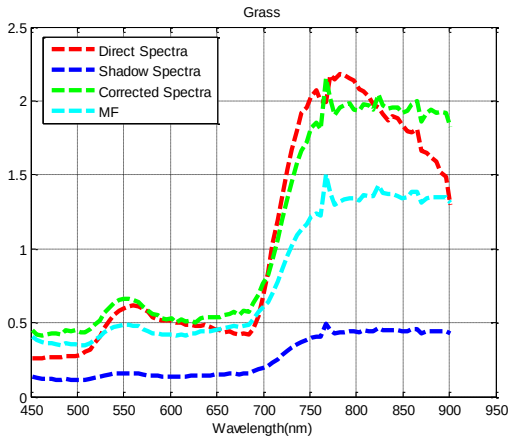

(c)

Figure 13 (a) the RGB image before correction (I_{NP}), (b) after correction and (c) the plot of shadow spectra before and after correction with respect to direct spectra.

Table 2 Spectra similarity of shadow reflectance before and after correction with respect to full illumination spectra for Field data.

Field Data	Before correction	Spectro-polarimetry technique	Ritcher MF technique
Angle Similarities	0.1047	0.0784	0.1047
Distance Similarities	0.2950	0.0533	0.0833

Table 3 Spectra similarity of shadow reflectance before and after correction with respect to full illumination spectra for Bunker data.

Bunker Data	Before correction	Spectro-polarimetry technique	Ritcher MF technique
Angle Similarities	0.1649	0.1349	0.1648
Distance Similarities	0.2722	0.0944	0.1414

6. Conclusion

This paper has presented a new method for illumination invariance and shadow correction on hyperspectral imageries. The spectro-polarimetry

technique is able to locate the shadow pixels by measuring the angle between vectors of the polarized and unpolarized images using SAM. The SAM values prove that direct and diffuse irradiance can be estimated using the polarizer technique. The correction shows an improvement on the shadow pixels for both indoor and outdoor scenes. Further improvement is needed particularly in direct and diffuse estimation for the development of a more robust shadow compensation algorithm.

Acknowledgement

This research was conducted as part of a 3 year PhD programme at DCMT, Cranfield University. The author would like to thank Malaysian Government for the scholarship to make this project possible. The second author would like to thank Drs C Lewis, R Bower & R Botton of the CPNI for the interest and partial support of this project. TC, KH and US would like to thank DCMT for the internal funding for the provision of studentships.

References

(1) Ibrahim, I., Yuen, P., Tsitiridis, A., Hong, K., Chen, T., Soori, U., Jackman, J., James, D. and Richardson, M. “Spectral consistensy on hyperspectral imageries.” *Defence S&T Technical Bulletin*, 2011: Vol. 4, 19:30.

(2) Hively W. D., McCarty G. W., Reeves III J. B., Lang M. W., Oesterling R. A. and Delwiche S. R. “Use of airborne hyperspectral imagery to map soil

properties in tilled agriculture fields." *Applied and Environmental Soil Science*, 2011: doi: 10.1155/2011/358193.

(3) Govender, M., Chetty, K. and Bulcock, H. "A review of hyperspectral remote sensing and its application in vegetation and water resource studies." April 2007: 145-152.

(4) Puckrin., E., Turcotte, C. S., Gagnon, M., Bastedo, J., Farley, V. and Chamberland, M. "Airborne infrared hyperspectral imager for intelligence, surveillance and reconnaissance applications." *Proc. of SPIE.* 2012. doi:10.1117/12.918251.

(5) Ray S. S., Singh J.P. and Panigrahy S. "Use of hyperspectral remote sensing for crop stress detection : Ground Based Studies." *International Archives of the Photogrammetry, Remote Sensing and Spatial Information Science*, 2010: 562-566.

(6) Tong, Q., Zhang, B., and Zheng, L. "Hyperspectral remote sensing technology and applications in China." *Proc. of the 2nd CHRIS/Proba Workshop, ESA/ESRIN.* Frascati, Italy, 2004.

(7) Freeman, J., Downs, F., Marcucci, L., Lewis, E. N., Blume, B. and Rish, J. "Multispectral and hyperspectral imaging: Applications for medical and surgical diagnostic." *Proceedings-19th International Conference - IEEE/EMBS.* Chicago, USA, 1997. 700-701.

(8) Carrasco, O., Gomez, R., Chainani, A. and Roper, W. "Hyperspectral imaging applied to medical diagnoses and food safety."

(9) Yuen, P. W. T. and Bishop, G. "Hyperspectral algorithm development for military applications: A multiple fusion approach." *3rd EMRS DTC Technical Conference.* Edinburgh, 2006.

(10) Driggers, R. G., Cox, P. and Edwards, T. *Introduction to infrared and electro-optical systems.* London: Artech house, 1999.

(11) Kruse, F.A., Kieren-Young, K.S. and Boardman, J.W. “Mineral mapping at Cuperite, Nevada with 63 channel imaging spectroradiometer.” *Photogramm. Eng. remote Sen.,*, 1990: 56, 83-92.

(12) Simpson, J.J. and Stit, R.S. “A procedure for the detection and removal of cloud shadow form AVHRR data over land.” *IEEE T Geosci. Remote Sens.* 1998. 36: 880-896.

(13) Ajtay, G.L., Ketner, P. and Duvingeaud. *Terretrial primary production and pytomass in the global carnon cycle.* New York: Wiley, 1982.

(14) Ibrahim, I., Yuen, P., Tsitiridis, A., Hong, K., Chen, T., Jackman, J., James, D. and Richardson, M. “Illumination independant object recognitions in hyperspectral imaging.” *SPIE Defence & Security.* Toulouse, France: Proceedings of the SPIE, 2010. 78380O-1-12.

(15) Mayer, R., Antoniades, J., Baumback, M., Chester, D., Edwards, J., Goldstein, A., Hass, D. and Henderson, S. “Shadowed onject detection for hyperspectral imagery.” *Proc. of SPIE: Infrared Spaceborne Remote Sensing and Instrumentation XV.* 2007. 66780L-1:11.

(16) Kao, H. and Ren, H. “A band ratio approach for classification in shaded area.” *ACRS2009.* 2009.

(17) Akiko, O. “Development of vegetation index using radiant spectra normlaized by their aritmetic mean.” *Proceedings of the Conference of the Remote Sensing Society of Japan.* Japan, 2006. vol. 40.

(18) Boardman, J.W., 1993, “Automated Spectral Unmixing of AVIRIS Data Using Convex Geometry Concepts,” in Summaries, Fourth JPL Airborne Geoscience Workshop, JPL Publication 93-26, v. 1, pp. 11-14.

(19) Fan, W., Hu, B., Miller, J. and Li, M. “Comparative study between a new nonlinear model and common linear model for analysing laboratory simulated-forest hyperspectral data .” *International Journal of Remote Sensing*, 2009: 2951-2962.

(20) Friman, O., Tolt, G. and Ahlberg, J. “Illumination and shadow compenstaion of hyperspectral images using a digital surface model and non-linear least squares estimation.” *Image and Signal Processing for Remote Sensing.* Proc. of SPIE, 2011. 81800Q-1: 8.

(21) Portigal, F., 2002, “Adaptive Reflectance Calibration” method; see http://www.ultraspectral.com

(22) Richter, R. and Muller, A. “De-shadowing of satellite/airborne imagery.” *International Journal Remote Sensing, 26:15*, 2005: pp 3137-3148.

(23) Adler-Golden, S.M., Matthew, M. W., Anderson, G. P., Felde, G. W., and Gardner, J. A., 2002, "An algorithm for de-shadowing spectral imagery", Proc. 11th JPL Airborne Earth Science Workshop, 5-8 March 2002, JPL-Publication 03-04, Pasadena, U.S.A.

(24) Richter, R. *Atmospheric/Topographic Correction for Satellite Imagery (ATCOR-2/3 User Guide).* German: German Aerospace Center, Version 6.1, January, 2005.

(25) Wolff, L.B. “Using polarization to separate reflection components.” *Proc. of IEEE Conf. Comput. Vision Pattern Recog. (CVPR).* San Diego: IEEE, June, 1989. 363-369.

(26) Egan, W. G. “Dark target retroreflection increase.” *Proc. of SPIE .* Denver, Colarado: SPIE, 1999. 218-225.

(27) Lin, S., Yemelyanov, K.M., Jr, E. N. P. and Engheta, N. “Separation and contrast enhancements of overlapping cast shadow components using polarization.” *Optic Express*, August 2006,: vol. 14, Issue 16, pages: 7099-7108.

(28) Wellems, D. and Bowers, D. “Improved hyperspectal imagery using diffuse illumination or a polarizer.” *Proc. of SPIE Vol. 7065, 706509.* 2008. 706509-1: 706509:9

(29) Shaw, G. and Burke, H. “Spectral imaging for remote sensing.” *Lincoln Laboratory Journal, vol. 14*, 2003: pp. 3-28.

(30) Suzuki, M., Takada, A., Yamada, T., Hayasaka, T., Sasaki, K., Takahashi, E. and Kumagai, S. “Low-reflectivity wire-grid polarizers multilayered by the glancing-angle-deposition technique.” *J. Nanophoton*, 2011: 5: 051501-1:9.

(31) Lin, S., Yemelyanov, K.M., Pugh, E. N. J. and Engheta, N. “Polarization-and Specular-Reflection-Based, Non-contact Latent Fingerprint Imaging and Lifting.” *Journal of Optical Society of America*, 2005: 2137-2153.

(32) Freeman, M. H. *Optics.* London: Butterworth, 1990.

(33) Zissis, G. J. *The infrared and electro-optic systems handbook.* Vol. Volume 1: Source of Radiation. Michigan, USA: IR Information Analysis Centre and SPIE Optical Engineering Press, 1993.

(34) Salekdeh, A. Y. *Mutispectral and hyperspectral images invariant to illumination.* Canada: Simon Fraser University Library, 2009.

(35) Richards, J. A. and Jia, X. *Remote sensing digital image analysis: An introduction.* Germany: Springer

(36) Randall, S.M. *Introduction to hyperspectral imaging.* Randall B. Smith: MicroImages, Inc., 2012, 2006.

(37) Ashton, E. A., Wemett, B.D., Leathers, R. A. and Downes, T. V. “A novel method for iilumination suppression in hyperspectral images.” *Proc of SPIE.* 2008. 69662C-1:69660C-8.

(38) Wolff, L. B. and Kurlander, D. J. “Ray tracing with polarization parameters.” *IEEE computer Graphics and Apllications,* 1990: 10: 44:55.

(39) Egan, W. G. Photometry and polarization in remote sensing. New York: Elsivier, 1985.

(40) Wolff, L., Nayar, S. K. and Oren, M. “Improved diffuse reflection models for computer vision.” *International Journal of Computer Vision* , 1998: 30 (1) : 55-71.

(41) Chang, Chein-I. *Hyperspectral Imaging: Techniques for Spectral Detection and Classification.* New York: Kluwer Academic/Plenum Publisher, 2003.